



**HAL**  
open science

## Thermo-mechanical stresses in cast steel dies during glass pressing process

Gilles Dusserre, Fabrice Schmidt, Gilles Dour, Gérard Bernhart

► **To cite this version:**

Gilles Dusserre, Fabrice Schmidt, Gilles Dour, Gérard Bernhart. Thermo-mechanical stresses in cast steel dies during glass pressing process. *Journal of Materials Processing Technology*, 2005, 162 (SI), pp.484-491. 10.1016/j.jmatprotec.2005.02.088 . hal-01716285

**HAL Id: hal-01716285**

**<https://hal.science/hal-01716285>**

Submitted on 6 Nov 2018

**HAL** is a multi-disciplinary open access archive for the deposit and dissemination of scientific research documents, whether they are published or not. The documents may come from teaching and research institutions in France or abroad, or from public or private research centers.

L'archive ouverte pluridisciplinaire **HAL**, est destinée au dépôt et à la diffusion de documents scientifiques de niveau recherche, publiés ou non, émanant des établissements d'enseignement et de recherche français ou étrangers, des laboratoires publics ou privés.

# Thermo-mechanical stresses in cast steel dies during glass pressing process

G. Dusserre\*, F. Schmidt, G. Dour, G. Bernhart

*CROME P, Ecole des Mines d'Albi-Carmaux, Route de Teillet, 81013 Albi Cedex 09, France*

---

## Abstract

Cast steel dies used in glass pressing process present an important dispersion in their lifetime in spite of apparently similar pressing parameters. In order to know if undetectable variations of any process parameter could produce such lifetime dispersal, a finite element simulation of glass pressing process is proposed. In this paper, glass is supposed to be a Newtonian fluid, the mould is considered as a thermo-elastic material, thermal transfer between glass and mould depends only on time and radiative heat transfer in glass is not taken into account. The validation of the results of this simulation is performed by comparison of the calculated pressing force and of the experimental one. Although the data introduced in the simulation are taken from the literature on the subject, the order of magnitude of the calculated pressing force is similar to the industrial one.

*Keywords:* Glass pressing process; Numerical simulation; Thermo-mechanical stresses; Cast steel dies

---

## 1. Introduction

Glass pressing is a forming process used to make hollow parts in only one stage (Fig. 1). The glass is heated up to 1500 °C in a furnace and then cooled around 1250 °C in the feeder. A gob is formed and it falls into the preheated lower mould. The glass flows then between the lower and the upper mould, activated by a hydraulic press. These tools are made of cast martensitic stainless steel GX30Cr13 (norm NF EN 10027-1 and Table 1). This process involves high temperature, high strain rate, thermal and mechanical stresses, fatigue phenomena, oxidation and complex shapes. They all lead to the formation of cracks on the lower mould surface. These cracks are mostly initiated on casting defects (shrinkage).

The lifetime of the mould is determined by the dimensions of these cracks: no defect must be visible on the finished part. It has been observed that the so defined lifetime could be very different (factor 2) between two moulds of the same batch, whereas the process parameters do not seem to have changed.

This paper presents a finite element simulation of the glass pressing process to calculate the thermo-mechanical stresses

in the dies. This simulation aims at identifying the process parameters for which small variation would involve significant stresses variation. The software FORGE2<sup>®</sup> was used because it authorizes a precise description of the kinematic of the process and possesses an automatic remeshing module. FORGE2<sup>®</sup> software is based on the finite element method. P1 + P1 linear triangular elements and an updated Lagrangian formulation are used. In order to minimize time calculation, a axisymmetrical simulation will be realized. The parameters that are meant to have the most important influence on the stresses in the mould are: the rheological behavior of glass, the mechanical behavior of the steel, the radiative and conductive heat fluxes in the glass, the heat flux density at gob/mould interface and the friction between glass and steel. It has been chosen to investigate this five parameters.

## 2. Input data of the simulation

### 2.1. Rheological behavior of glass

The glass under study is Pyrex<sup>®</sup> (Table 2). It is a borosilicate glass with a low expansion coefficient in order to resist thermal shocks up to 300 °C.

---

\* Corresponding author.

*E-mail address:* gilles.dusserre@enstimac.fr (G. Dusserre).

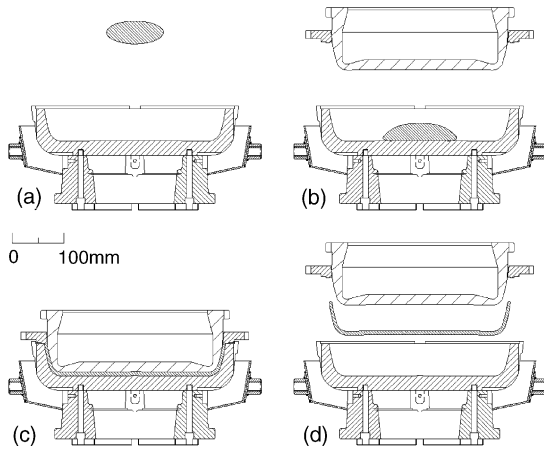


Fig. 1. Main stages of the glass pressing process: (a) delivery, (b) pressing, (c) pressure maintenance and (d) takeout.

Table 1

Chemical composition (wt.%) of GX30Cr13 steel

C	0.3
Cr	13
Si	0.6
Mn	0.9
Ni	<0.5

The rheological behavior of glasses is very temperature dependant [1]. At low temperature, glass behaves like a brittle elastic solid; around the glass transition temperature, it behaves like a thermo-rheological simple visco-elastic material [2–4]; and at high temperature it behaves like a thermo-dependent viscous fluid [5–7].

Non-Newtonian behavior is observed [8] as the viscosity of the glass melt decreases with an increase of strain rate. Nevertheless in this paper, glass will be assumed to be a Newtonian fluid (Eq. (1)), that means that the viscosity varies only with the temperature as described by the Vogel–Tammann–Fulcher (VTF) equation (cf. Eq. (2) and Fig. 2) [9]. This equation is only valid at temperatures over 900 °C, but it will be assumed that below this temperature the glass is almost rigidified and does not flow anymore

$$\underline{\underline{s}} = 2\eta(T)\underline{\underline{\dot{\epsilon}}} \quad (1)$$

$$\log \eta = A + \frac{B}{T - T_0} \quad (2)$$

Table 2

Chemical composition (wt.%) of Pyrex® glass [21]

SiO <sub>2</sub>	82.57
B <sub>2</sub> O <sub>3</sub>	10.81
Na <sub>2</sub> O	5.13
Al <sub>2</sub> O <sub>3</sub>	1.23
K <sub>2</sub> O	0.13
CaO	0.05
MgO	0.05
TiO <sub>2</sub>	0.02
FeO	0.01

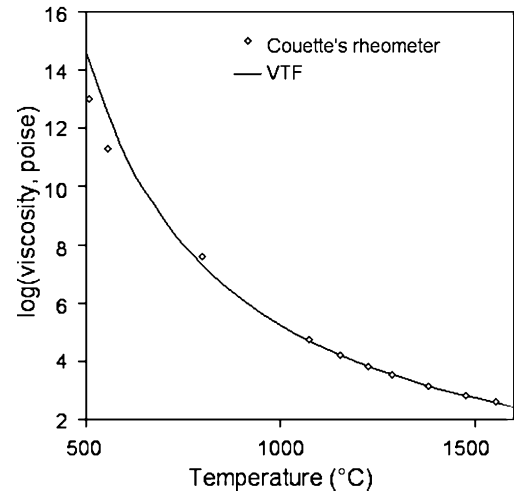


Fig. 2. Temperature dependency of the viscosity of Pyrex®: experimental points and VTF equation (with  $A$ ,  $B$  and  $T_0$  given in Table 3).

Table 3

Values of coefficients of Pyrex® glass TVF equation (viscosity in poise and temperature in °C)

$A$	−1.6007
$B$	5931.3
$T_0$	134

where  $\underline{\underline{s}}$  is the deviatoric part of the Cauchy stress tensor,  $\eta$  is the glass viscosity,  $\underline{\underline{\dot{\epsilon}}}$  is the strain rate tensor,  $T$  is the temperature and  $A$ ,  $B$ ,  $T_0$  are constants given in Table 3.

## 2.2. Mechanical behavior of GX30Cr13 steel

It will be assumed that the steel of the mould behaves as a thermo-elastic solid. Young's modulus is introduced in the software FORGE2® as a function of temperature (Fig. 3) and the Poisson ratio is set to the usual 0.3.

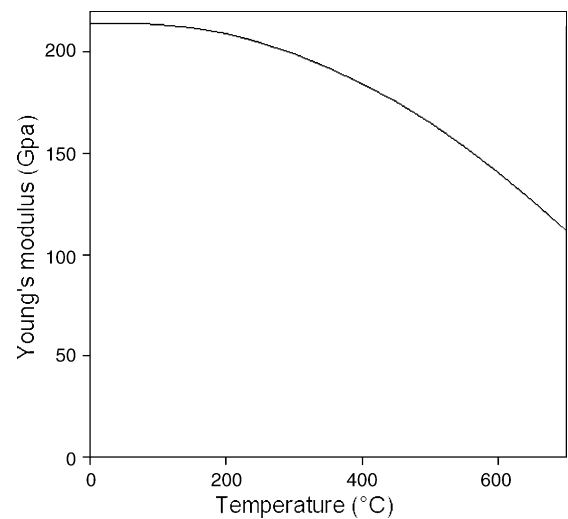


Fig. 3. Young's modulus of GX30Cr13 steel as a function of temperature.

Table 4  
Values of coefficients of glass conductivity (temperature in °C) [10]

$C_1$ ( $\text{W m}^{-1} \text{ }^\circ\text{C}^{-1}$ )	0.7222
$C_2$ ( $\text{W m}^{-1} \text{ }^\circ\text{C}^{-2}$ )	0.001583

### 2.3. Conductive and radiative heat transfer in glass

The high temperature dependency of the glass rheological behavior involves the necessity of a precise thermal computation. Glass being a semi-transparent media, heat transfer occurs not only by conduction but also by radiation. The thermal conductivity of glass is supposed to vary linearly with temperature as described by Loulou et al. (cf. [10] and Eq. (3)). Experimental data missing, the values of the constants  $C_1$  and  $C_2$  are taken to be the same as in [10] (see Table 4)

$$k_{\text{cond}} = C_1 + C_2 T \quad (3)$$

Radiative heat transfer is a phenomena hard to model because heat flux in one point of the gob is influenced by every other points of the glass part. The easiest way to take the radiative heat transfer into account is to use a diffusion approximation: a radiative conductivity is defined as a function of the temperature, radiative and conductive heat fluxes are then calculated by Fourier's law. An expression of this radiative conductivity  $k_{\text{rad}}$  was proposed by Rosseland [11] (Eq. (4) and Fig. 4)

$$k_{\text{rad}}(T) = \frac{16n^2\sigma}{3\bar{\kappa}_{\text{Ross}}(T)} T^3 \quad (4)$$

$$\frac{1}{\bar{\kappa}_{\text{Ross}}(T)} = \frac{\int_0^\infty \frac{1}{\kappa(\nu)} \frac{\partial B(\nu, T)}{\partial T} d\nu}{\int_0^\infty \frac{\partial B(\nu, T)}{\partial T} d\nu} \quad (5)$$

where  $n$  is the refractive index of the semi-transparent media,  $\sigma$  is the Stefan–Boltzmann constant,  $T$  is the temperature in  $K$  and  $\bar{\kappa}_{\text{Ross}}$  is the Rosseland mean extinction coefficient defined by Eq. (5).  $\nu$  is the frequency of the radiation,  $\kappa(\nu)$  is the

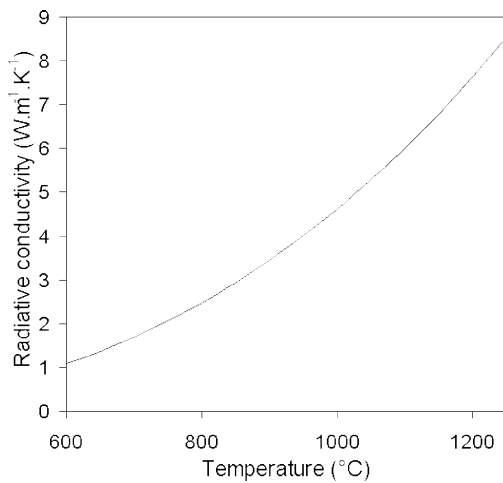


Fig. 4. Rosseland radiative conductivity of Pyrex<sup>®</sup> as a function of temperature, computed with  $n=1.47$ ,  $\kappa(\nu)=654.7 \text{ m}^{-1} \forall \nu \in [5.52 \times 10^4 \text{ Hz}, 7.72 \times 10^4 \text{ Hz}]$ ,  $\kappa(\nu)=9.16 \text{ m}^{-1} \forall \nu \in [7.72 \times 10^4 \text{ Hz}, 9.44 \times 10^4 \text{ Hz}]$  and  $\kappa(\nu)=52.68 \text{ m}^{-1} \forall \nu \in [9.44 \times 10^4 \text{ Hz}, 7.91 \times 10^8 \text{ Hz}]$ .

extinction coefficient and  $B(\nu, T)$  is the blackbody intensity as described by the Planck's law.

This method is easy to compute, but it is based on the assumption that the glass is optically thick. This means that most of the radiation is absorbed in the neighborhood of the particle that emitted it. This assumption is not valid for a glass domain with small dimensions, as in the present case.

An analytical solution of the Radiative Transfer Equation is available in a one-dimensional case, but it requires to know the optical properties of the glass and the surface of the mould, and strong assumptions are made on the geometry of the problem [10,12].

Numerical methods could be used such as discrete ordinate method, improved diffusion approximation, ray tracing, Monte Carlo [13], but they require long calculation time, incompatible with our objectives.

Fig. 5 presents the profile of heat flux divergence in the glass supposed to be an infinite plate with a thickness of 9 mm (intermediate thickness of the dish during pressing), for a computed temperature profile with a high temperature gradient around the boundaries, as calculated with the Rosseland diffusion approximation, the analytical method [10,13] and without any radiation effects. One can observe that the Rosseland method over evaluates the heat flux divergence compared to the analytical method. This figure shows that radiative heat flux divergence is important, especially in the middle of the glass where conductive heat flux divergence is negative whereas radiative heat flux divergence is positive. In a first step, it will be chosen to assume that radiative heat transfer could be neglected compared to conductive heat transfer because analytical and numerical methods are not easy to introduce in FORGE2<sup>®</sup> software, and Rosseland diffusion approximation is not valid.

### 2.4. Heat flux density at gob/mould interface

The second function of a mould being to cool the glass, the thermal computation requires to know the heat flux den-

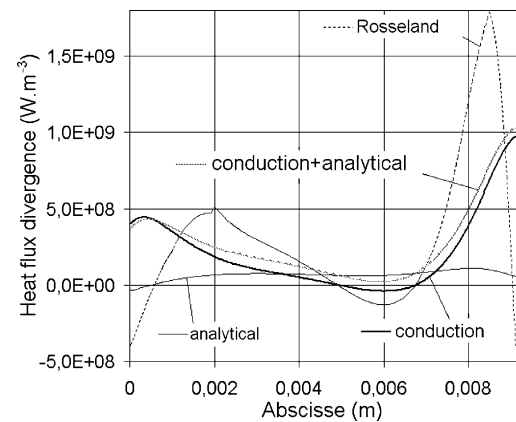


Fig. 5. Comparison of profile of heat fluxes divergence in the one-dimensional case for Rosseland diffusion approximation, analytical method and without radiation.

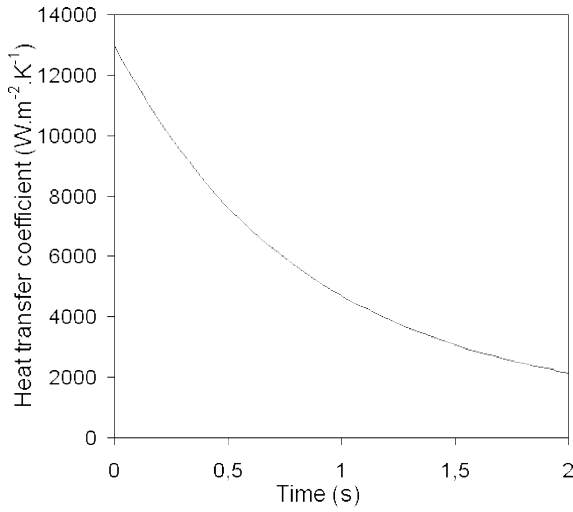


Fig. 6. Heat transfer coefficient at glass/mould interface as a function of time [15].

sity exchanged between the gob and the mould. Experiments have been reported in literature [10,14,15] to measure heat flux at the glass/mould interface as a function of time. Semi-empirical models have been developed by decoupling radiative and convective parts of the flux. For example, Pchelyakov [10,16–18] proposed a heat transfer coefficient equal to the conductivity divided by the thickness of a gap between gob and mould. In this paper we prefer to use the experimental results of Moreau et al. [15] as depicted in Fig. 6.

### 2.5. Friction between glass and mould

Friction between glass and steel is greatly influenced by the temperature of the glass at the interface. Studies were led on friction between glass and steel in the condition of delivery gobs into moulds [19]. Li et al. [20] investigated the influence of temperature and strain rate on the friction at the interface during compression test of titanium rings lubricated with glass. Below 950 °C, strain rate does not seem to play a significant role on the friction behavior. These results will be used in this paper: it is supposed that glass temperature at the interface is 750 °C, and that friction behavior follows the Tresca model with a friction factor  $\bar{m}$  equal to 0.28 (cf. [20]). In the present case, FORGE2<sup>®</sup> software describes the Tresca model as in Eq. (6),  $\tau$  is the shear stress and  $\Delta\vec{V}$  is the difference between the velocity of the glass and the velocity of the mould

$$\tau = -\bar{m}\eta(T)\frac{\Delta\vec{V}}{\|\Delta\vec{V}\|} \quad (6)$$

### 2.6. Heat capacity of Pyrex<sup>®</sup>

The heat capacity of Pyrex<sup>®</sup> is introduced in FORGE2<sup>®</sup> software as a function of the temperature as described by Richet et al. [21].

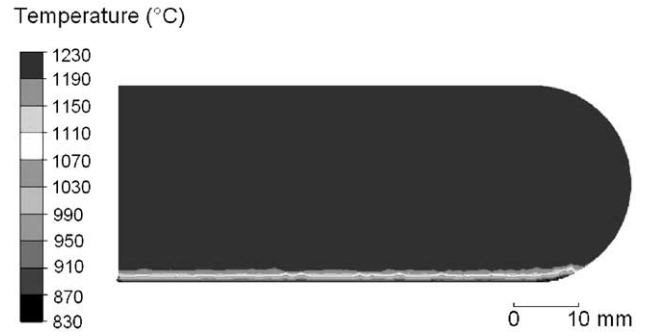


Fig. 7. Initial condition of the gob for the loading stage.

## 3. Simulation of the gob loading into the mould

### 3.1. Initial conditions

The first stage of the glass pressing process that has been chosen for simulation is loading step of the gob into the mould. The initial gob shape and temperature distribution are presented in Fig. 7. It represents the cooling due to the short contact of the gob with the sliding channel (heat transfer coefficient set to classical value 2000 W m<sup>-2</sup> K<sup>-1</sup>) during the transfer from the feeder to the mould and air at 25 °C (heat transfer coefficient 150 W m<sup>-2</sup> K<sup>-1</sup> [22]). The gob has been placed at a distance of 50 mm from the mould and falls freely. To perform such simulation, the initial mesh contains 728 triangular nodes. The initial shape and temperature distribution of the mould are shown in Fig. 8. The initial temperature distribution is the result of a 30 s cooling by convection in free air (heat transfer coefficient 10 W m<sup>-2</sup> K<sup>-1</sup>) corresponding to the time between loading the mould on the press and first pressing. The initial mesh contains 2518 nodes.

### 3.2. Boundary and interfacial conditions

Thermal exchanges considered are convection with air during gob loading, convection between the mould and air, and thermal exchanges between mould and glass. The heat transfer coefficient between the gob and air is equal to 150 W m<sup>-2</sup> K<sup>-1</sup>, as it could be interpolated at 1100 °C from the results of the inverse method proposed by Lochegnies and

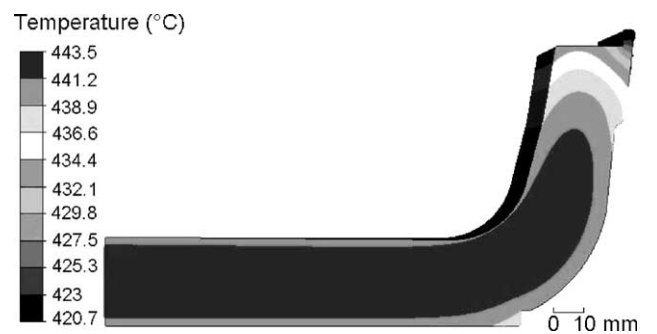


Fig. 8. Initial condition of the mould for the loading stage.

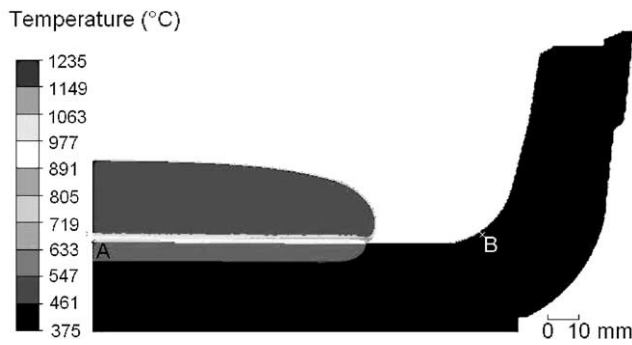


Fig. 9. Initial temperature distribution for the pressing stage.

Marechal [22]. Convection coefficient between air and steel as been set to  $10 \text{ W m}^{-2} \text{ K}^{-1}$  (a classical value for natural convection between steel and calm air) eat transfer coefficient as been defined as a function of time (Section 2.4 and Fig. 6).

Friction between glass and steel is defined in Section 2.5.

### 3.3. Results

The total time of the simulation is 2 s corresponding to the actual waiting time before pressing starts. CPU time calculation is 6 min 4 s. The final configuration of this simulation will be defined as initial configuration of the next pressing stage (Fig. 9). Fig. 10 presents the variation of the Von Mises equivalent stress at the surface of the mould on the axis (Fig. 9, point A) during gob loading simulation and Fig. 11 shows the temperature at the same point. The maximum Von Mises equivalent stress reaches 430 MPa at  $515^\circ\text{C}$  (the maximum temperature reached is  $520^\circ\text{C}$ ). Mechanical behavior of GX30Cr13 cast steel should be studied in details, but it could be supposed, that this stress could at least induce local plastic deformation in the shrinkage zones

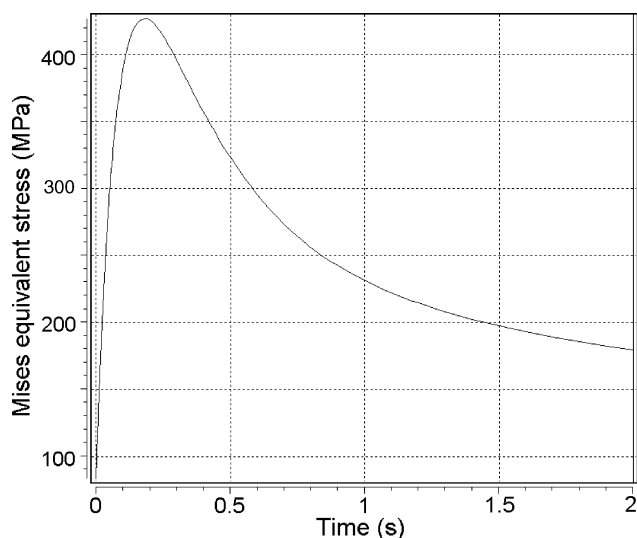


Fig. 10. Evolution of Mises equivalent stress at the surface of the mould with time during gob loading.

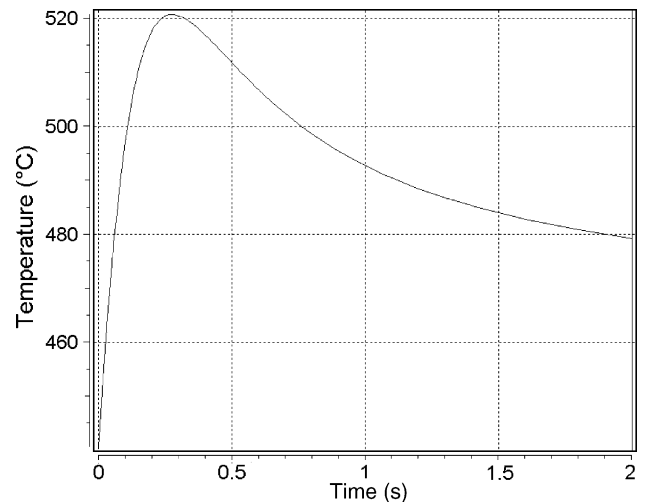


Fig. 11. Evolution of temperature at the surface of the mould with time during gob loading.

where stress concentration may occur, and lead to cracks appearance.

## 4. Simulation of the pressing stage

### 4.1. Initial conditions

The second stage of the process to be simulated is pressing. The initial configuration corresponds to the final one of the gob loading stage. Fig. 9 shows the initial temperature distribution in the gob and in the lower mould. Initial temperature of the upper mould has been set to an uniform value ( $250^\circ\text{C}$ ).

### 4.2. Boundary conditions

The boundary conditions for this simulation are the same as for gob loading, except the heat transfer coefficient between gob and moulds is now set to a constant value ( $2000 \text{ W m}^{-2} \text{ K}^{-1}$ ). It has indeed been supposed that pressure has little effect on heat transfer coefficient and that its value is the final one of the gob loading stage (Fig. 6). The inner surface of the upper mould is cooled by a  $20^\circ\text{C}$  water flow (with a heat transfer coefficient set to  $20,000 \text{ W m}^{-2} \text{ K}^{-1}$ ).

### 4.3. Press piloting

The lower mould is fixed and the upper one is moved according to the height–time curve (Fig. 12). This curve has been interpolated from initial height, final height and initial velocity with an exponential function.

### 4.4. Validation of the computation

In order to validate this numerical computation with experimental data, computed pressing force has been com-

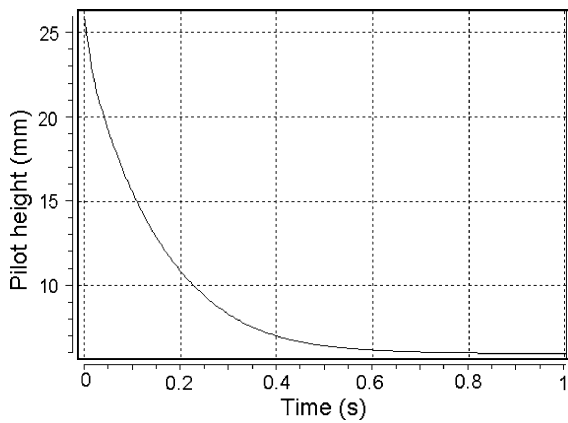


Fig. 12. Piloting height as a function of time.

pared with the real one (the maximal force of the industrial hydraulic press). The calculated force has been plotted in Fig. 13. Some numerical accident due to calculation restarts may explain the five instants where the force is null. Although the models that have been introduced in the software are not very accurate (radiative heat transfers neglected) or correspond to conditions that are not exactly similar to the ones of our case (values from the literature), the order of magnitude of the computed pressing force does not reach the maximum value of the real press and seems to be coherent. It could be expected that the force increase up to a maximum value before to stabilize at this value. The difference between the calculated and the expected pressing force could be explained by the piloting of the press in the pressing simulation which does not correspond to measurement (the velocity is not described on a realistic way).

#### 4.5. Results

CPU time calculation is 24 h and 15 min 8 s for a 1 s simulation. The final temperature distribution in gob and moulds is shown Fig. 14. The Von Mises equivalent stress at the surface of the mould on the axis (Fig. 9, point A) has been plotted as a function of time in Fig. 15a and temperature at the same

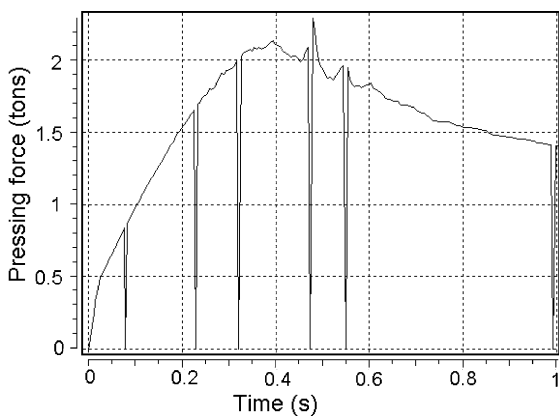


Fig. 13. Computed pressing force as a function of time.

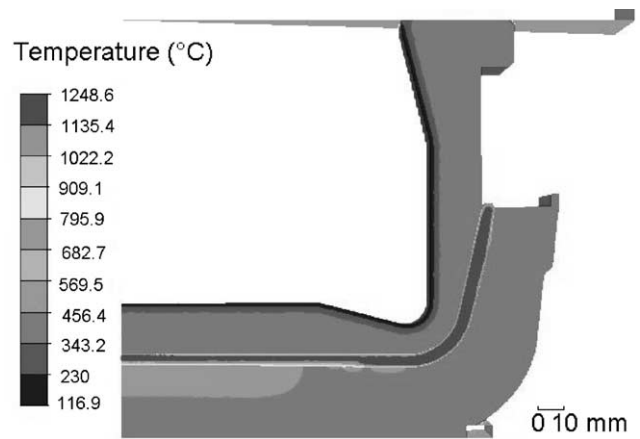


Fig. 14. Temperature distribution in gob and moulds at the end of pressing.

point in Fig. 16. The maximum Von Mises equivalent stress is 162 MPa at 502 °C. As it could be seen in Fig. 17, there is other zone where stresses are important (in the edge of the plane surface of the mould: Fig. 9, point B). At this location, maximum Von Mises equivalent stress is not so important as on the axis but a high stress level exists (106 MPa at 494 °C). The evolution of the stress at this point during pressing is

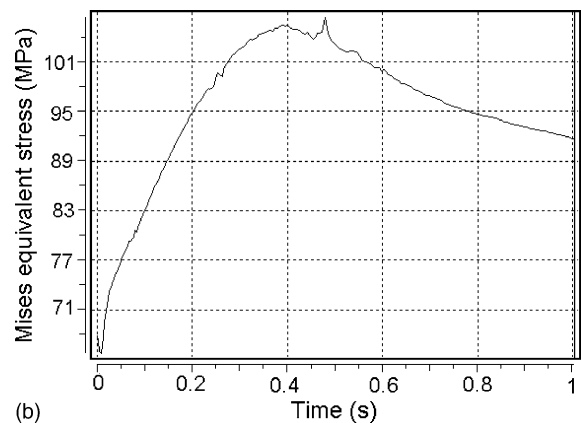
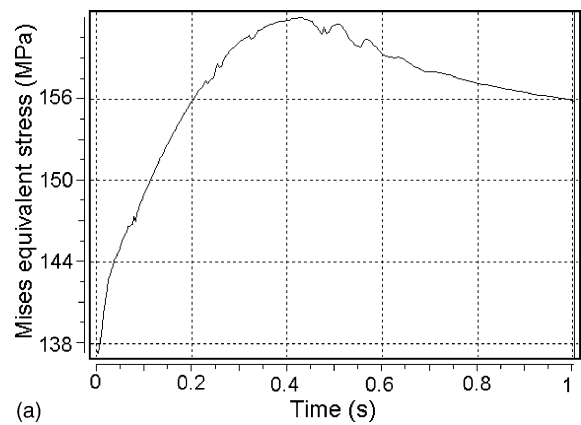


Fig. 15. Evolution of Mises equivalent stress at (a) point A and (b) point B with time during pressing.

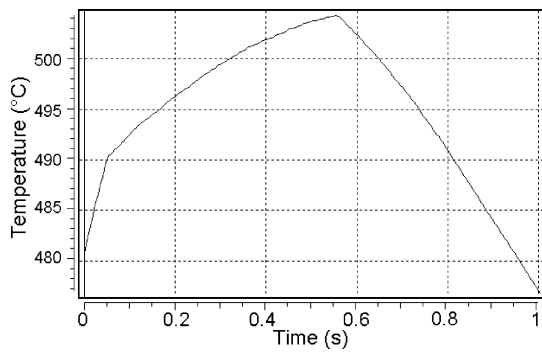


Fig. 16. Evolution of temperature at the surface of the mould with time during pressing.

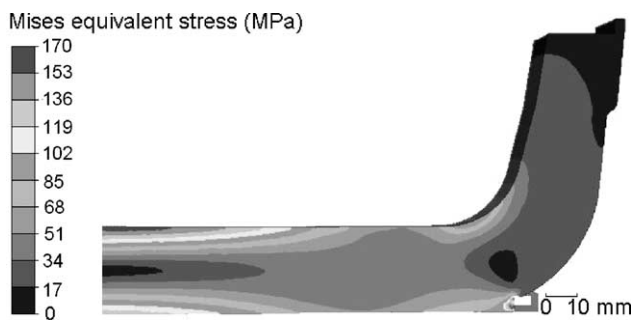


Fig. 17. Mises equivalent stress distribution in lower mould during pressing.

plotted Fig. 15b. One can observe in Fig. 17 that between the two zones previously mentioned, the stress level is not so high. It could be concluded that as for loading stage, plastic deformation could occur around the shrinkages during pressing but stress level is not so elevated as during gob loading.

## 5. Conclusion

In agreement with the computed Mises equivalent stress distribution, it could have been observed that cracks appearance could occur at two locations in the mould: at the center or at the edge of the plane surface. The first zone is solicited both thermally and mechanically, whereas the second one is solicited mostly mechanically. Industrial moulds present cracks in one or the other of these two zones depending on the shape of the mould: few proof and axisymmetrical moulds are damaged at the center whereas proof and elliptical moulds are damaged at the edge of the plane surface.

More investigations could be led to valid the calculated stress distribution in the mould more accurately as with the pressing force of the industrial process. For example, laboratory pressing tests could be led on a compression test machine to measure accurately the pressing force and the displacement of the upper mould with time. A simplest mould shape and temperature measurements with thermocouples could allow to evaluate heat fluxes at glass mould interface and to valid the thermal computation in the mould. Instrumentation of an industrial mould with thermocouples is also forecasted.

This simulation could be improved by taking experimental data into account (glass rheology, mechanical behavior of GX30Cr13 steel, heat flux density at the gob/mould interface, piloting of the press, etc.) and by taking radiative heat fluxes into account, and then be used to study the influence of process parameters on moulds lifetime (initial glass and mould temperature, pressing velocity, etc.). Others mould materials could also be tested.

## Acknowledgements

The present investigation has been carried out with the financial support of Aubert et Duval, Newell S.A and Saint-Gobain SEVA.

## References

- [1] J. Zarzycki, *Glasses and the Vitreous State*, Cambridge University Press, 1991.
- [2] P. Wiertel, D. Locheignies, J. Oudin, Optimization techniques for flat glass tempering, in: *Proceedings of the Colloquium on Modelling of Glass Forming Processes*, Valenciennes, France, 1998, pp. 219–227.
- [3] H. Hessekenper, R. Brückner, Elastic constants of glass melts above the glass transition temperature from ultrasonic and axial compression measurements, *Glastechnische Berichte* 64 (2) (1991) 29–38.
- [4] M. Van Iseghem, L. Fourment, J.F. Agassant, Residual stress simulation in a glass/metal contact, in: *Proceedings of the Colloquium on Modelling of Glass Forming Processes*, Valenciennes, France, 1998, pp. 253–261.
- [5] D. Locheignies, C. Marion, E. Carpentier, J. Oudin, Finite element contributions to glass manufacturing control and optimization. Part 2. Blowing, pressing and centrifuging of hollow items, *Glass Technol.* 37 (5) (1996) 169–174.
- [6] A. Milutinović-Nikolić, R. Jančić, R. Aleksić, Mathematical modelling and simulation of drawing thin glass sheet from a rectangular perform, *Glass Technol.* 39 (5) (1998) 166–172.
- [7] M. Hyre, A. Leven Harrison, Effect of feeder design and operation on gob shape, *Verre* 9 (2) (2003) 20–23.
- [8] Y. Yue, R. Brückner, On the different descriptions of the non-Newtonian viscosity (shear-thinning effect) of glass melts with respect to heat dissipation, *Glastechnische Berichte* 69 (6) (1996) 179–185.
- [9] A. Sipp, D.R. Neuville, P. Richet, Viscosity, configurational entropy and relaxation kinetics of borosilicate melts, *J. Non-Cryst. Solids* 211 (1997) 281–293.
- [10] T. Loulou, R. Abou-Khachfe, J.P. Bardon, Estimation de la résistance thermique de contact durant la solidification du verre, *Int. J. Therm. Sci.* 38 (1999) 984–998 (in French).
- [11] S. Rosseland, Note on the absorption of radiation within a star, *Monthly Notices R. Astron. Soc.* 84 (1924) 525–528.
- [12] S. André, V. Manias, B. Rémy, M. Lazard, D. Maillet, A reduced analytical model for solving heat transfer in glasses, in: *Proceedings of the Colloquium on Modelling of Glass Forming Processes*, Valenciennes, France, 1998, pp. 47–54.
- [13] B.J. van der Linden, R.M.M. Matheij, M. Slobt, Radiative heat transfer in hot glass melts, in: *Proceedings of the Colloquium on Modelling of Glass Forming Processes*, Valenciennes, France, 1998, pp. 95–108.
- [14] D. Locheignies, C. Noiret, C. Thibaud, J. Oudin, Computation procedure for the temperature in hot glass. Application to the finite

- element simulation of hollow glass forming, *Glass Sci. Technol.* 69 (8) (1996) 253–264.
- [15] P. Moreau, S. Grégoire, D. Locheignies, Experimental methodology for the determination of the heat transfer coefficient at the glass/mould interface, *Verre* 9 (2) (2003) 24–27.
- [16] R. Viskanta, J. Lim, Analysis of heat transfer during glass forming, *Glass Sci. Technol.* 74 (11/12) (2001) 341–352.
- [17] K. Storck, D. Loyd, Heat transfer modeling of the parison forming in glass manufacturing, *Glass Technol.* 39 (6) (1998) 210–216.
- [18] E. Brauns, J. Patyn, Finite element calculation of thermomechanical stresses in candidate ceramic components for press and blow moulds, *Glass Technol.* 40 (2) (1999) 58–64.
- [19] M. Falipou, F. Sicloroff, C. Donnet, New method for measuring the friction between hot viscous glass and metals, *Glass Sci. Technol.* 72 (3) (1999) 59–66.
- [20] L.X. Li, D.S. Peng, J.A. Liu, Z.Q. Liu, Y. Jiang, An experimental study of the lubrication behavior of A5 glass lubricant by means of the ring compression test, *J. Mater. Process. Technol.* 102 (2000) 138–142.
- [21] P. Richet, M. Ali Bouhifd, P. Courtial, C. Téqui, Configurational heat capacity and entropy of borosilicate melts, *J. Non-Cryst. Solids* 211 (1997) 271–280.
- [22] D. Locheignies, C. Marechal, Inverse determination of glass viscosity and heat transfer coefficient by industrial testing, *Glass Sci. Technol.* 75 (6) (2002) 304–312.